



HAL
open science

Thermal behavior of grain-oriented electrical steel wound core solid-state transformer

Houssam Ichou, Daniel Roger, Mathieu Rossi

► **To cite this version:**

Houssam Ichou, Daniel Roger, Mathieu Rossi. Thermal behavior of grain-oriented electrical steel wound core solid-state transformer. *COMPEL: The International Journal for Computation and Mathematics in Electrical and Electronic Engineering*, 2022, 10.1108/COMPEL-06-2021-0223 . hal-03587272

HAL Id: hal-03587272

<https://hal.science/hal-03587272>

Submitted on 29 Nov 2023

HAL is a multi-disciplinary open access archive for the deposit and dissemination of scientific research documents, whether they are published or not. The documents may come from teaching and research institutions in France or abroad, or from public or private research centers.

L'archive ouverte pluridisciplinaire **HAL**, est destinée au dépôt et à la diffusion de documents scientifiques de niveau recherche, publiés ou non, émanant des établissements d'enseignement et de recherche français ou étrangers, des laboratoires publics ou privés.

Thermal behavior of Grain-Oriented Electrical Steel wound core Solid-State Transformers

Houssam Ichou

Univ. Artois, UR 4025, Laboratoire Systèmes Électrotechniques et Environnement (LSEE),
F-62400 Béthune, France

Daniel Roger

Univ. Artois, UR 4025, Laboratoire Systèmes Électrotechniques et Environnement (LSEE),
F-62400 Béthune, France

Mathieu Rossi

Univ. Artois, UR 4025, Laboratoire Systèmes Électrotechniques et Environnement (LSEE),
F-62400 Béthune, France

Abstract

Purpose – The grain oriented electrical steel (GOES) is a soft magnetic material able to operate at high flux densities and high temperatures. The paper propose new design of high power compact solid state transformers (SSTs), made with a wound GOES core, that benefits of the natural reduction of iron losses at high temperatures.

Design/methodology/approach - An experimental approach, coupled with numerical and analytical investigations, are widely used for proving the validity of the proposed concept of a high power medium frequency transformer.

Findings – With high temperatures cores, compact high-power SSTs can be designed with basic converter structures. Compared to the existing technologies, the proposed design opens the way toward compact SSTs operating at much larger powers with similar efficiencies.

Research limitations/implications – The main issue consists in controlling the core temperature, which must be much higher than the coil one.

Practical implications - The increasing number of intermittent renewable sources places the electric grid stability at risk. Smart nodes, made of SSTs, improve the global grid stability because they are able to provide a real-time control of energy fluxes at critical points. In railway applications, SST cells can be distributed along the train providing a lager volume for passengers.

Originality – The paper proves that the design of high-power transformers with a GOES wound core much hotter than coils is possible. It proposes also a thermal equivalent circuit that helps the design.

Social Implications - The increasing part of renewable and intermittent sources in the production of electricity require performant and high power SSTs made with components that have an environmental foot print as low as possible.

Keywords: Transformers, Thermal design, Iron losses, Eddy currents, Soft magnetic materials.

I. INTRODUCTION

The compactness of SST cells and the possibility to split high power SSTs in several compact cells is a major advantage for railway traction applications (Dujic et al., 2012; Zhao et al., 2012). Each SST cell provides the required galvanic insulation and output and the voltage change with a medium frequency transformer. The SST design is made for maximizing the power density and the efficiency while respecting material limits (temperature, flux density, electric stress in the insulation system). Currently, most of available SSTs operate at high frequencies, over 10 kHz, with transformer cores made of ferrite (Garcia et al., 2016), nanocrystalline (Elrajoubi and Ang, 2019; Ozdemir et al., 2017) or amorphous materials (Du et al., 2010).

The paper describes an alternative solution for high power SSTs operating at medium frequencies, in the kHz range. For such medium frequencies, the transformer can be built around a GOES wound core. Such cores can

operate at high peak flux densities (Lemaître and Belgrand, 2014). It is also proved that, at medium frequencies, the eddy current losses in GOES thin sheets are lower for square voltages than for sine ones, for the same frequency and peak flux density (Hamdinou, 2018). Consequently, the converter topologies can be very simple (one pulse per half period) offering low switching losses (Ichou et al., 2019). The sheets are covered on both faces of a thin mineral insulation layer these inorganic layers can operate at very high temperatures. A GOES wound core can operate up to 500°C, without any significant decrease of the saturation flux density (Ababsa et al., 2028). The resistivity increases naturally with the temperature, which corresponds to a decrease of core losses.

The main goal of the paper is to test the possibility of manufacturing a compact high-power transformer, operating at medium frequency, with a GOES core much hotter than the coils. The approach is mainly experimental. A medium frequency transformer prototype was placed in a standard electrical cabinet. It is placed in the air flow of a fan and connected between two electronic converters. The experimental results are interpreted with a nodal thermal equivalent circuit.

II. MODULAR STRUCTURE FOR HIGH POWER SOLID-STATE TRANSFORMERS FOR RAILWAY APPLICATIONS

A simple way for building high-power SSTs consist in connecting several elementary SST cells together for sharing voltages currents and powers. Figure 1 shows an example of high-power modular SST for railway applications. In Europe, several train feeding systems exist; this diversity is due to historic reasons. The highest voltage 25 kV / 50 Hz corresponds to the lowest catenary currents (Steimel, A., 1996). In figure 1, the bidirectional rectifier provides the high voltage DC bus that feeds the modular SST. The output is the on board 1500 V DC bus used by the train traction and auxiliary systems. On the HV side, the cells are connected in series for sharing the HVDC while they are connected in parallel for adding currents. For a 25 kV catenary voltage, the maximum voltage of the HVDC bus is $25\sqrt{2} = 35.4 \text{ kV}$. With input converters built with insulated gate bipolar transistors (IGBTs) rated at 6.5 kV (Infineon products, 2021) for each cell, the SST can be made of 7 cells for reaching the DC bus voltage with a safety margin of 10 kV. The SST control system must provide a good balance of the voltage between the cells. The output converters can be made of 3.3 kV IGBT.

Similar modular high-power SSTs can be used for connecting a 3-phase medium voltage grids to solar power plants, wind farms, local smart grids and many other applications of similar voltages and powers.

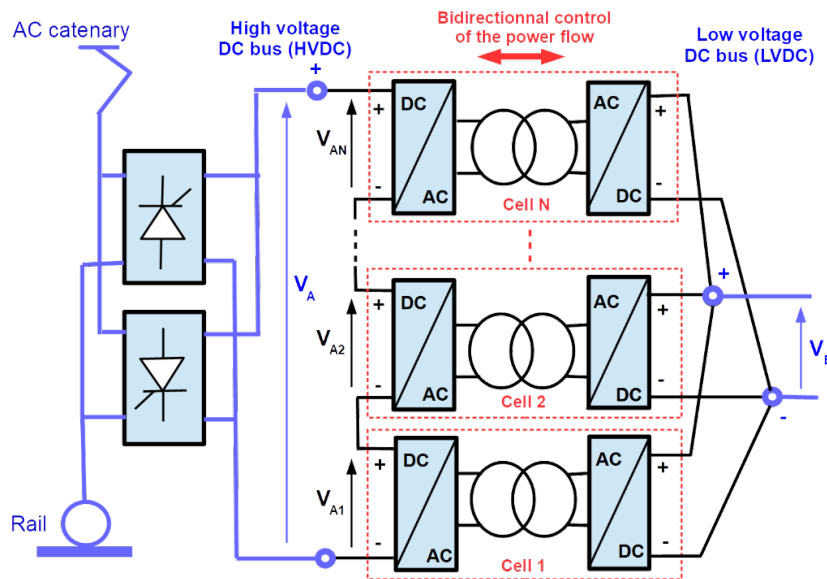


Fig.1. Example of high power modular SST in railway applications.

The heart of each SST cell is a medium frequency transformer (MFT) that provides the voltage change and the galvanic insulation between the AC catenary and the on-board DC bus. Fig. 1 shows that the electrical insulation system (EIS) of the transformer of the cell N, at the top of the stack, withstands the full input voltage V_A between the primary coil and the and the core. This common-mode voltage is the peak value of the catenary voltage (35.4kV). This high common-mode stress is also applied to the DC/AC converter of the cell; this converter must be insulated from the grounded metallic frame of the whole SST. The IGBT command signals must be transmitted by optical fibers capable of providing the required galvanic isolation.

Figure 2 extracts the upper cell of the modular structure and presents the converters. For such high-power applications, the frequency is limited because of the switching losses in IGBTs. The transformer can be designed for medium frequencies, in the kHz range. The medium frequency transformer (MFT) is placed between two identical bridges made of IGBTs operating with one pulse per half period for limiting the switching losses.

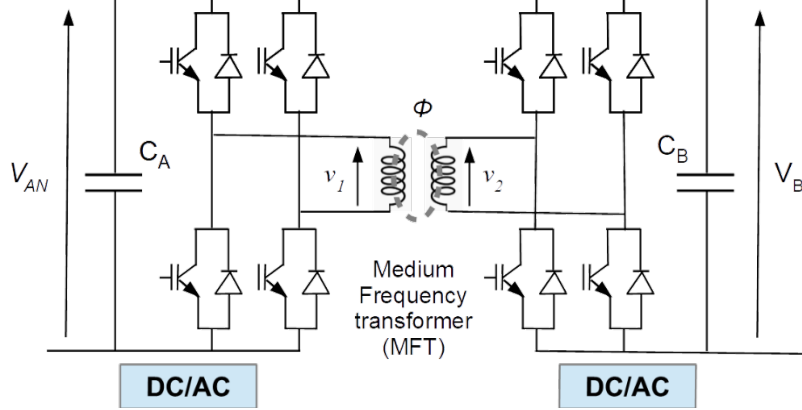


Fig.2. Structure of a SST cell: a medium frequency transformer is placed between two IGBT bridges.

This structure, called “dual active bridge (DAB)” (Nan and Ayyanar, 2013; Feng B. et al, 2014). The filtering capacitances C_A and C_B must be large enough for limiting variations of V_{AN} and V_B during a period. Noting ω the angular frequency imposed by the command, L_l the leakage inductance of the MFT and φ_N the phase lag between the command signals of the two IGBT bridges, the average power P_N transmitted by the cell N is given by (1) for a full wave command.

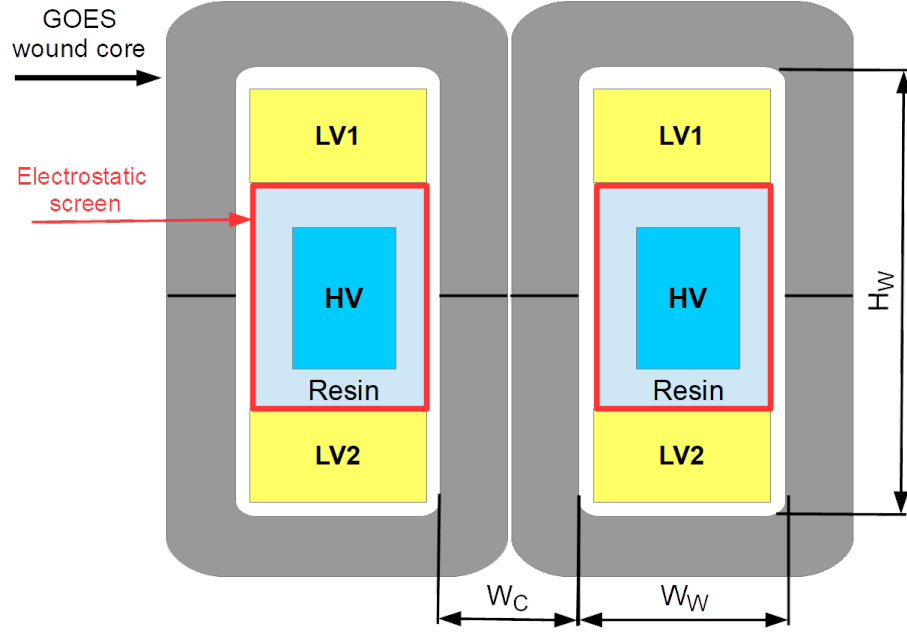
$$P_N = \frac{V_{AN} V_B}{\pi L_l \omega} \varphi_N (\pi - |\varphi_N|) \quad (1)$$

For given voltages V_{AN} and V_B , the maximum transferred power is obtained for $\varphi_N = \pm \pi/2$. Most of the time, the catenary feeds the train and the command variable φ_N is positive. However, the energy flow can be reversed during slow down operations tuning φ_N at a negative value. The expression (1) shows that the product $L_l \omega$ limits the maximum power. Consequently, the leakage inductance must be as low as possible, which implies a reduced leakage flux in the MFT.

III. HIGH POWER MEDIUM FREQUENCY DRY-TYPE TRANSFORMER STRUCTURE

For standard dry-type transformer technologies, the common-mode insulation between a coil and the core is made of several insulation layers: the enameled wire thin polymer layer, the insulating support used for winding the coil, the impregnating varnish and the residual air near the core. The insulating materials have a higher relative permittivity than air; therefore, the electric field is concentrated in the residual air layer. Unfortunately, the dielectric strength of air layers is low (about 3 kV/mm for dry air); with this technology it is difficult to get high common mode voltages in a reasonable air thickness. On the other hand, thicker air layer increases the leakage inductance. Faced with such a dilemma, the standard solution is the transformer immersed in oil to benefit the high dielectric strength of oil. The paper proposes an alternative dry-type transformer structure (Fig. 3). The high-voltage (HV) coil is placed inside a metallic box filled with a high dielectric strength insulating resin (16 kV/mm). The metallic box acts as an electrostatic shield that concentrates the common-mode electric field inside the resin. The box is connected to the transformer core for canceling the electric field in the air between the core and the electrostatic shield. After hardening the resin, a narrow slit is made along the box for avoiding to make an unwanted short-circuited turn around the core. With such a structure and a minimum distance of 5 mm between the enameled wire and the metallic box, the expected common-mode voltage capability is over the required value of 35.4 kV . This very high common-mode voltage requires a careful process ensuring a correct filling of the box without air voids in the resin.

The low leakage inductance is obtained by splitting the low voltage coil in two half coils (LV1, LV2) placed on both side of the HV one. With this structure a large part of the magnetic field lines inside the core window crosses the primary and the secondary coils; flux is as low as possible. The EIS of the LV coils is standard because the maximum common-mode voltage is only 1500 V , the standard dry-type transformer technology can be used.



$$A_W = H_W \cdot W_W$$

$$A_C = W_C \cdot (\text{core depth in z-direction})$$

Fig.3. MFT structure able to provide a high commode voltage insulation of the HV coil and a low leakage inductance.

Generally speaking, the apparent power S of a transformer depends on the area of the window that the core gives to the windings A_W , the area of the core for the magnetic flux A_C , the window filling factor K_F , the RMS current density in the coils J_{RMS} , the maximum value of the flux density B_m and the frequency f (McLyman C., 2017). The general expression (2) can also be used for a transformer fed by square voltages when the coefficient 4.44 is changed to 4 (Hamdinou S., 2019). Consequently, for a given frequency, the core must operate to the highest possible flux density, considering acceptable core losses.

$$S = [4.44 K_F A_W A_C J_{RMS} B_m f]^{3/4} \quad (2)$$

A large core windows area A_W is interesting but it corresponds to long average magnetic field lines. The high magnetic permeability of the core allows to keep a reasonable magnetizing current with a large core window. A recent paper presents a state of the art on advanced ferromagnetic materials in power electronic converters (Rodriguez-Sotelo D. et al., 2020). The authors note that few soft magnetic materials have the required high permeability and high saturation flux density. The best candidates are the amorphous or nano crystalline thin ribbons and the FeSi grain oriented electrical steel (GOES). In order to offer industrial perspectives, the reasonable choice of the GOES is made because wide strips are easily available for building the large wound cores of the transformers of high-power SST cells.

Figure 4 shows the experimental HV coil made with a high thermal conductivity epoxy resin and heatsinks that increase the direct flux from the coil to the external airflow, improving cooling. This figure shows also the high common-mode voltage coil connections and the GOES wound core offering large windows. The wound core made of two identical half cores built by winding a thin GOES strip on a support that imposes the shape of the window. After the annealing thermal cycles, the support is removed, and the half core is cut for allowing the coil insertion. The cutting planes are machined for obtaining a very flat surfaces and a minimum magnetic gap. At any point of the two half cores, the magnetic field is tangent to the GOES strip, in the material rolling direction that corresponds to the easy magnetisation axis providing the maximum magnetic permeability and saturation flux density. The thin GOES strip ($165 \mu m$) is covered of thin insulating layers ($3 - 5 \mu m$) on both faces. This coating is composite: an additional layer of phosphate glass is applied on the magnesia silicate which is formed during the grain growth process (IEC 60404-1-1, 2004). The coating is able to withstand the temperature of $840^\circ C$ reached during annealing. The coating imposes a tensile stress, obtained during cooling. This stress has a beneficial magnetostrictive effect on losses (Beckley Ph., 2000). The crystalline structure of the GOES is very stable (Xia Z. et al., 2008; Lemaître R. and Belgrand T., 2014).

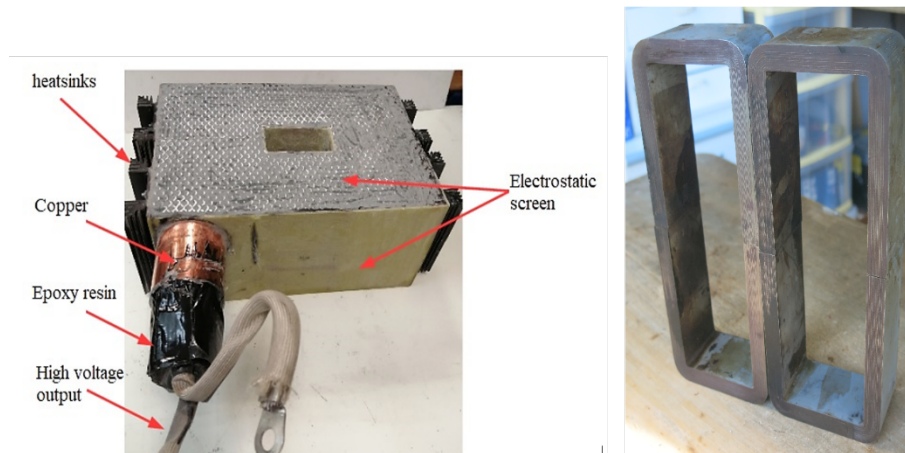


Fig.4. HV coil inside its electrostatic shield and large windows wound GOES magnetic core.

IV. TRANSFORMER GOES WOUND CORE BEHAVIOUR

A recent study, which uses an Epstein frame able to operate at high temperatures, presents hysteresis loops of GOES strips measured up to 600° (Ababsa M.L et al., 2018). Figure 5, extracted from this paper, shows these loops for 400 Hz sine voltages. These experimental results shows that the areas of hysteresis loops are lower and lower when the temperature increases. Consequently, the global core losses decrease with temperature. These loops show also that the GOES saturation flux density at 500 A/m, which is 1.8 T at 20°C decreases at 1.5 T at 500°C. The reduction is stronger over 500°C; therefore, the GOES can be used up to 500°C.

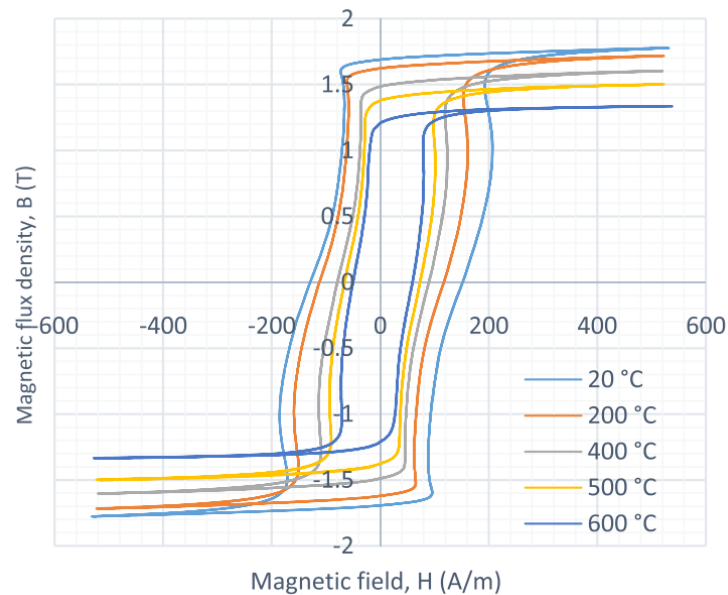


Fig. 5. Hysteresis loops of GOES strips measured up to 600°C with a sine voltage at 400 Hz (Ababsa M.L and Ninet O. and Velu G. and Lecoite J.P. (2018), "High-Temperature Magnetic Characterization Using an Adapted Epstein Frame," *IEEE Transactions on Magnetics*, vol. 54, pp. 1-6, 6 2018. DOI: 10.1109/TMAG.2018.2811727).

The variations of core losses with frequency can be modelled by Bertotti's equation (Bertotti G., 1988). This method splits the core losses in three parts: the quasi-static losses, the eddy current losses, and the excess losses. This well-known analysis is defined for sine voltages and for a negligible skin effect in a strip. Over 1 kHz and for 165 μm thick high permeability GOES strips, the skin effect cannot be neglected. A complementary analysis has been made considers only eddy current losses because the importance of this phenomenon increases with frequency. This analysis uses a non-linear numerical time-stepping finite element analysis applied to a small part of a strip of the GOES wound core (Hamdinou, 2018). In this work, the instantaneous eddy current losses $p(t)$ are computed from the current density $J(x, t)$ at any point inside the GOES strip of thickness a . This quantity is given by (3) where l is the half-core average length, N_s the number of strips and b their width. The temperature variation is taken into account considering the material resistivity increase with the temperature given by (4) where ρ_{20} is the GOES

resistivity at 20°C ($0.48 \cdot 10^{-6} \Omega \cdot m$), the core temperature and α the material temperature coefficient ($22 \cdot 10^{-3} K^{-1}$). The static B(H) curve is supposed unchanged.

$$p(t) = N_s l b \int_{-\frac{a}{2}}^{\frac{a}{2}} \rho J^2(x, t) dx \quad (3)$$

$$\rho = \rho_{20}[1 + \alpha(T - 20)] \quad (4)$$

Figure 6 presents the simulation results obtained for rectangular voltage at a 2 kHz. The voltage imposes a triangular flux, which peak value corresponds to an average flux density is 1.3 T. The left graph presents the distribution of the local flux density inside a strip at a time corresponding to the same peak average flux density (1.3T). The blue line corresponds to a resistivity at 20°C and the green one at 260°C. It can be seen that the increase of the resistivity changes deeply the local flux density distribution inside a strip; at 20°C, the flux density at the sheet borders reach the saturation. The right graph presents the synthesis of 7 simulations made with resistivity corresponding to temperatures between 20°C and 260°C. Each point is obtained computing the mean value of $p(t)$, given by (3). These simulations show that eddy current losses are strongly reduced when the core temperature increases. These results open perspectives for designing medium frequency transformers with GOES wound cores at a higher temperature than coils. The coils must remain cold because copper resistivity increase a negative effect on the copper losses. For designing such a transformer, the thermal behavior of the whole structure is a key point that must be studied and verified experimentally.

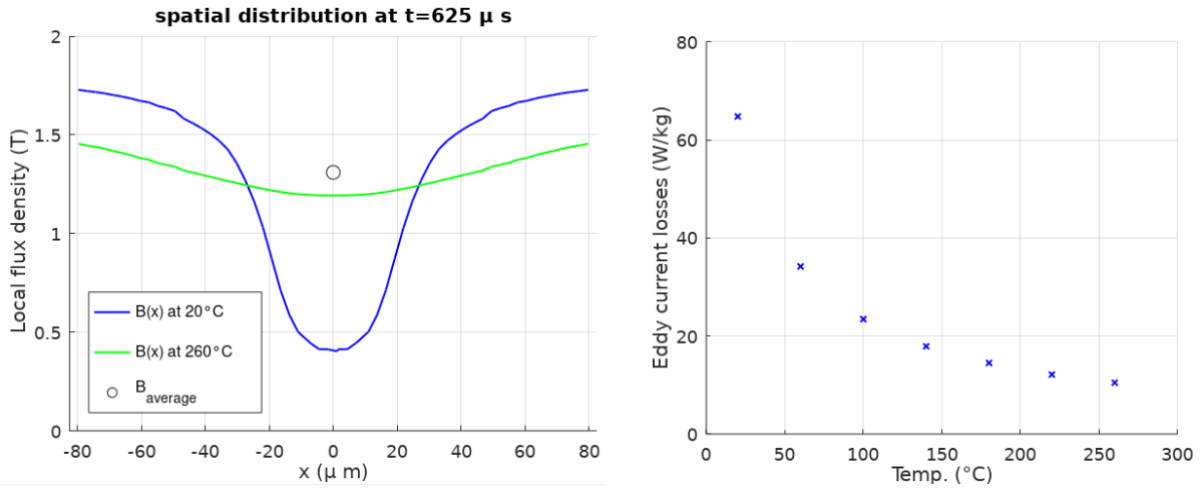


Fig. 6. Simulations results at a peak average flux density of 1.3 T at 2 kHz for square voltage (left: spatial distribution of the flux density inside a GOES strip; right: specific eddy current losses).

V. PROTOTYPE OF A HIGH-POWER SST CELL BASED ON A GOES WOUND CORE TRANSFORMER

A prototype has been made for studying the thermal behavior of the medium frequency transformer presented in Fig. 3 placed in the SST cell defined on Fig. 2. A picture of the SST cell is presented in Fig. 7. The HV bridge is made with 3.3 kV IGBT legs and the appropriate insulated gate driver (Thalheim, J., 2008). The LV bridge is made with standard 1200V/400A IGBT legs.

The transformer coils are cooled by heatsinks placed in the vertical air flux or the fan. The high-voltage coil is made of 66 turns of Litz wire made of 43 enameled strands of 0.85 mm. The secondary winding is made with two 16-turn coils connected in series made of similar Litz wire (86 strands of 0.85). The transformation ratio is 0.483.

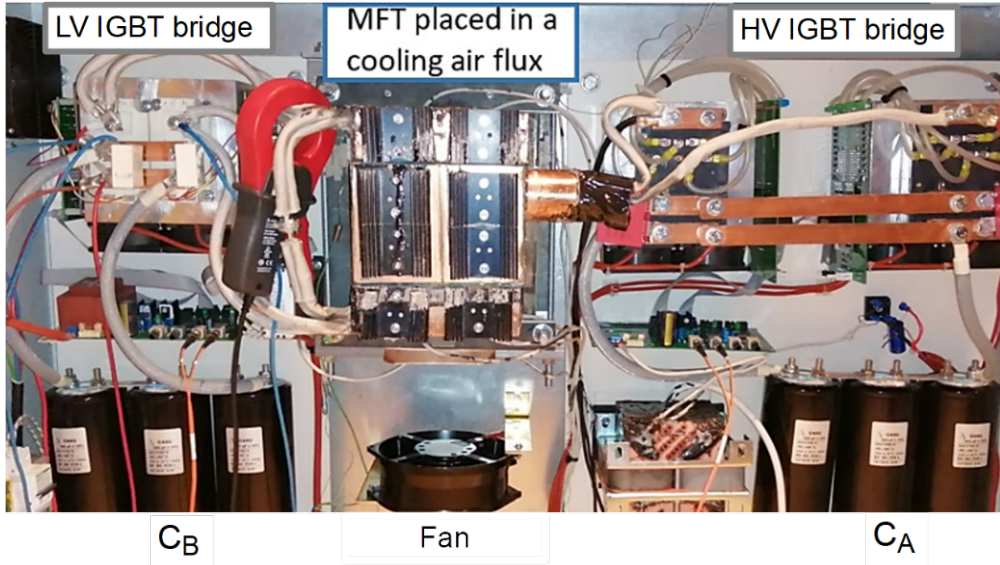


Fig. 7. Prototype of SST cell made of a hot-core medium-frequency transformer placed in a cooling air flux and two IGBT bridges in an electrical cabinet.

1. Thermal model of the medium frequency transformer

The thermal equilibrium is reached when the heat produced by the losses is equal to the heat transferred to the ambient air. These phenomena are modelled by the equivalent circuit of the left part of Fig. 8. The discretization is made by splitting the transformer in 5 elements assumed to be at the same temperature as shown on the right part of Fig. 8. The thermal resistances are supposed independent of temperature (linear model). The GOES core is modelled by two nodes: the central core (cc) and the two lateral cores (lc) supposed to be at the same temperature because of the transformer's symmetry. The capacitances represent the thermal inertia of the transformer parts; they are calculated multiplying the element mass by the specific heat of the material. For the coils, only the copper masses are considered because copper masses are much larger than the resin ones and the copper specific heat is higher. The numerical values are given in table I.

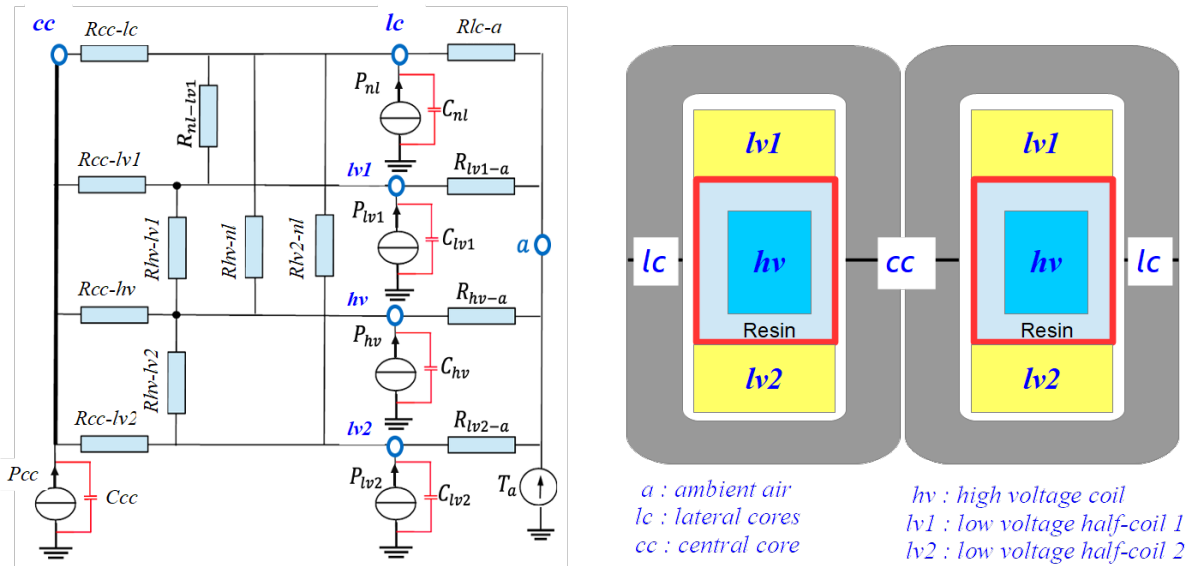


Fig.8. Nodal equivalent circuit used as thermal model and node positions.

Table I. Thermal capacitances of elements.

Element	Central core (cc)	Lateral cores (lc)	HV coil (hv)	LV1 coil ($lv1$)	LV2 coil ($lv2$)
Mass (kg)	2.27	3.6	6.8	3.3	3.3
Specific heat ($J g^{-1} K^{-1}$)	0.805	0.805	0.38	0.38	0.38
Thermal capacitance ($kJ K^{-1}$)	1.83	2.9	2.6	1.26	1.26

The central core is hotter than lateral cores because it has no direct contact with the air flow. The heat flowing from the central core toward the two lateral cores is modelled by the thermal resistance R_{cc-lc} . This resistance is calculated considering the 4 thermal paths from the center of cc to the two centers of lc . The elementary resistance of each path is computed by (5) where S_k is the area offered to the heat flux in the path k , d_k the average length of the path and λ_k the thermal conductivity of the material.

$$R_k = \frac{d_k}{\lambda_k S_k} \quad (5)$$

The thermal resistances R_{cc-hv} , $R_{cc-lv1,2}$ represent the heat transfers between the central core and the 3 coils. They correspond also to conduction phenomena. The heat flux crosses an air layer and a polymer one for reaching the copper that corresponds to the node. These thermal resistances are computed with (5) considering a single path with the same area S_k offered to the thermal flux in the two materials with their own thermal conductivity. The right part of figure 8 shows that there is no direct path joining $lv1$ and $lv2$. However, thermal exchanges exist between the central coil and the other ones. These resistances are computed with the same method. Results are presented in table II considering a 1 mm thick air layer between the coils and the core.

Table II. Resistances corresponding to thermal conduction phenomena inside the transformer.

Material	λ ($Wm^{-1}K^{-1}$) Thermal conductivity	R_{cc-hv} (K/W) Central core - HV coil	$R_{hv-lv1,2}$ (K/W) HV coil - LV coils	$R_{lc-lv1,2}$ (K/W) Lateral core - LV coils	R_{lc-hv} (K/W) Lateral core - HV coil	$R_{cc-lv1,2}$ (K/W) Central core - LV coils	R_{cc-lc} (K/W) Central core - Lateral cores
Air	0.0262	1.07	0.11	3.22	3.25	2.65	
Epoxy resin	0.66	0.42	0.21	0.13	0.65	0.21	
Total for the EIS		1.49	0.32	3.35	3.90	2.86	
Electrical steel	26						9.2

The 4 thermal resistances on the right part of the nodal circuit ($R_{lv1,2-a}$, R_{hv-a} and R_{lc-a}) correspond to the heat transfer to the air flow of the fan. These thermal resistances corresponding to convection phenomena are estimated experimentally. A power is injected successively in each coil by a DC current. The corresponding IGBT bridge operates as a chopper. Figure 9 shows an example of voltage and current waveforms. The chopper is tuned to very small duty cycles (2.5%). On this figure, it can be seen that the current ripple is about 12 A peak-to-peak for a mean value of 150 A. The current harmonics are much lower than the mean value; they can be neglected for calculating the mean power, which reduces to the product of the voltage and current mean values.

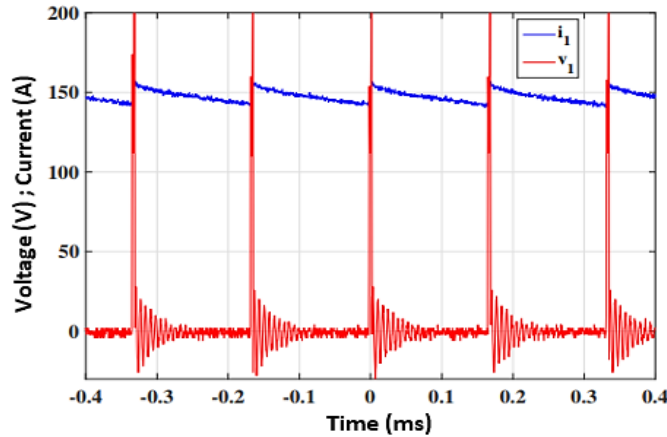


Fig.9. Current and voltage waveforms for a LV coil during the DC test.

The copper temperature is determined by (6) from the DC resistance obtained by dividing the mean voltage by the mean current. In (6), the copper temperature coefficient is $\alpha = 3.9 \cdot 10^{-3} K^{-1}$, the ambient temperature is T_0 and R_0 the resistance measured at ambient temperature. The experimental results presented in table III are made at steady state and for an ambient temperature $T_0 = 20^\circ C$.

$$T = T_0 + \frac{1}{\alpha} \left[\frac{R_{DC}}{R_0} - 1 \right] \quad (6)$$

Table III. DC tests experimental measurements.

DC fed coil	P_{cc} (W)	P_{lc} (W)	P_{hv} (W)	P_{lv1} (W)	P_{lv2} (W)	T_{lc} (°C)	T_{hv} (°C)	T_{lv1} (°C)	T_{lv2} (°C)	T_a (°C)
HV	0	0	553	0	0	35	92			20
LV1 and LV2	0	0	0	375	375	34		67	67	20

The exploitation of these results are made using the equivalent circuit of the left part of Fig. 8 and the thermal resistances values of table II. The 4 unknown thermal resistances are determined by successive simulations for each line of table III with SPICE a circuit simulator. Table IV shows the 4 unknown thermal resistances measured when the transformer is placed in the electrical cabinet presented in Fig. 7

Table VI. Thermal resistances corresponding to the convection phenomena.

R_{nl-a} (K/W)	R_{lv1-a} (K/W)	R_{lv2-a} (K/W)	R_{hv-a} (K/W)
0.4	0.16	0.16	0.35

2. Test of the SST cell at no load

Measurements at no load are made for testing the medium frequency transformer with rectangular voltages when the copper losses are much lower than the core ones. The SST cell is supplied on the high voltage side. This voltage and the frequency impose the peak value of the average flux density in the core B_m , which is determined by (7). V_A is the DC input voltage imposed to the cell, $N_1 = 66$ is the number of turn of the HV coil, $A_C = 12.4 \text{ cm}^2$ is the area offered to the magnetic flux and f the frequency.

$$B_m = \frac{V_A}{4 N_1 A_C f} \quad (7)$$

Figure 10 shows two core losses measurements as a function of the average temperature of the core for operating points corresponding to at 3 kHz/0.8 T (blue line) and at 2 kHz/1.3 T (green line).

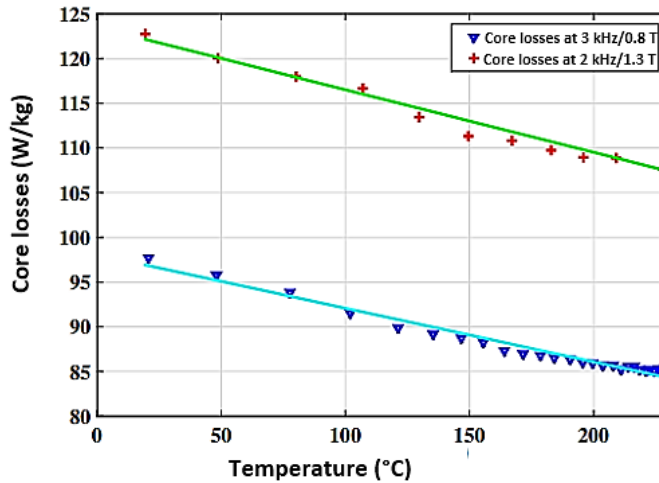


Fig.10. Core losses variations with the core average temperature for to operating points.

The core losses decrease with temperature. Comparing the experimental curve at 1.3 T/2 kHz with the eddy current losses obtained by simulation (Fig. 6 - right), it can be seen that eddy currents losses are more or less half the total core losses at ambient temperature. At higher temperature, this ratio becomes lower but the total losses decrease with temperature.

2. Prototype test at low load

For on-load tests, the SST cell, is fed by a DC source that imposes the voltage V_{IN} ; a load on connected at the output (Fig. 11). The input voltage V_{IN} is set to 620 V and the frequency to 2 kHz. The electronic load imposes the output voltage whatever the current ($V_{OUT} = 320V$). The power transferred by the SST cell is tuned by the angle φ , following (1). This test case corresponds to an actual use of a SST connected between two DC grids imposing the two voltages while the currents depend on the SST command φ .

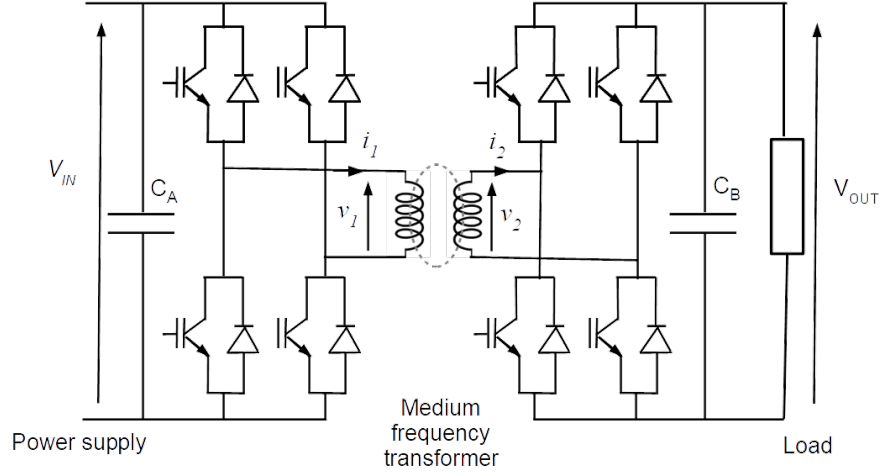


Fig.11. On-load test of the SST cell.

Figure 12 gives the waveforms of the voltages v_1 (blue line) v_2 (black line) and the current i_1 (red line). The phase lag command of the output bridge relatively to the input one is $\varphi = 8^\circ$. For this operating point, the current RMS values are $I_{1RMS} = 11.7 A$ and $I_{2RMS} = 24.1 A$.

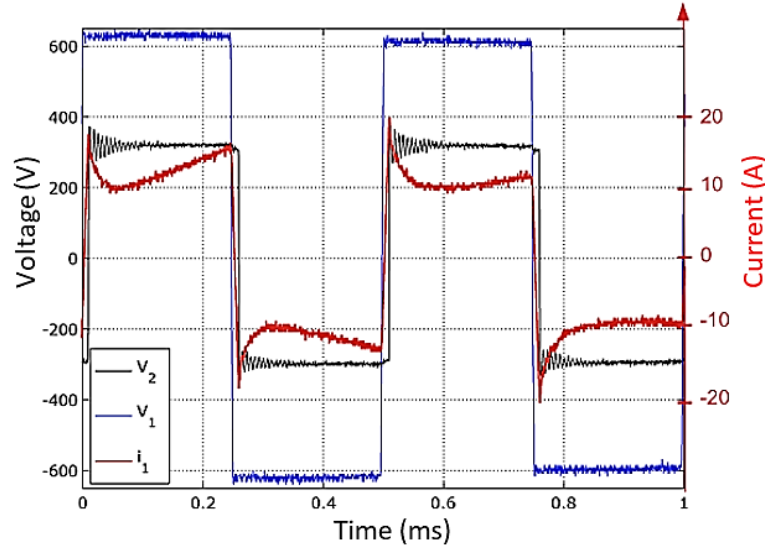


Fig.12. Voltages and current waveforms recorded during the test at low load.

The operating point of this test is used as input data for computing the temperatures with the thermal equivalent circuit presented in section V.1. With a constant angle φ , the currents and the voltages remain constant because of the voltage regulation of the electronic load. The copper losses increase with the coil temperatures because of the natural increase of the copper resistivity (copper $\alpha = +3.9 \cdot 10^{-3} K^{-1}$). The powers at the starting point are computed with the RMS currents at the coil resistances measured at 2 kHz and at $20^\circ C$. Conversely, the losses in the central and lateral cores decrease with their temperatures. This phenomenon is modelled by a linear approximation of the specific core losses $P_s = a(T - T_a) + b$ measured during the test at no load ($a = -0.07 W \cdot kg^{-1} \cdot K^{-1}$ and $b = 87 W/kg$). The power sources P_{CC} and P_{LC} are determined considering the masses and temperatures of the corresponding elements. A SPICE solver is used for computing the temperatures at the nodes of the thermal equivalent circuit. In this model, temperatures are represented by voltages. Each power source represented by two current sources connected in parallel : a constant one for the losses at $20^\circ C$ and a voltage-dependent one representing the variations of the core and copper losses with the temperature at the corresponding nodes. Simulation results and measured temperatures are plotted in Fig. 13 for the GOES core.

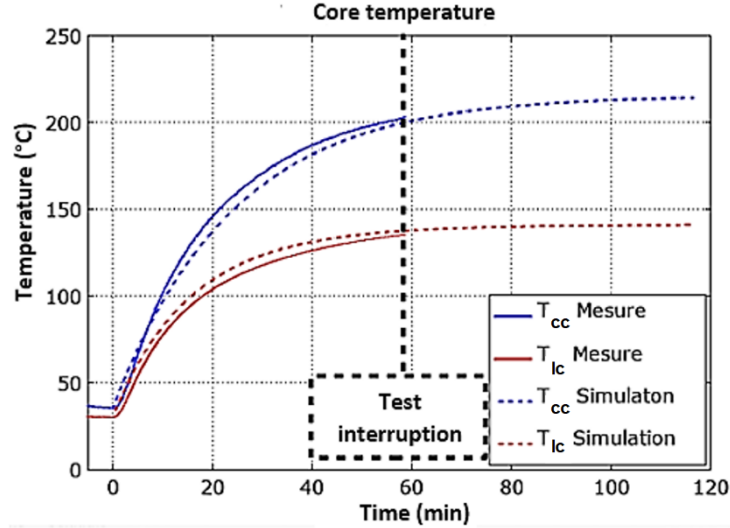


Fig.13. Core temperatures: measurements and simulations.

The test has been stopped at $t = 55 \text{ min}$ for security reasons, before thermal steady state. At $t = 55 \text{ min}$, the temperature inside the resin was over its temperature class at a measurement point. Moreover, the smell around the SST cell was typical of a coil over its thermal capabilities. However, Fig. 13 shows a good concordance between core temperature measurements and the values predicted by the thermal model during a large part of the transient state. It can also be seen that the central core is much hotter than the lateral ones.

Temperature measurements in the encapsulating resin were made during this test. The right part of figure 14 shows the position of thermocouples placed at half the thickness of an LV coil. The left part of this figure shows the measured temperatures. The red curve (thermocouple T8) denotes a temperature over the thermal class of the resin (155°C) at $t=55 \text{ min}$.

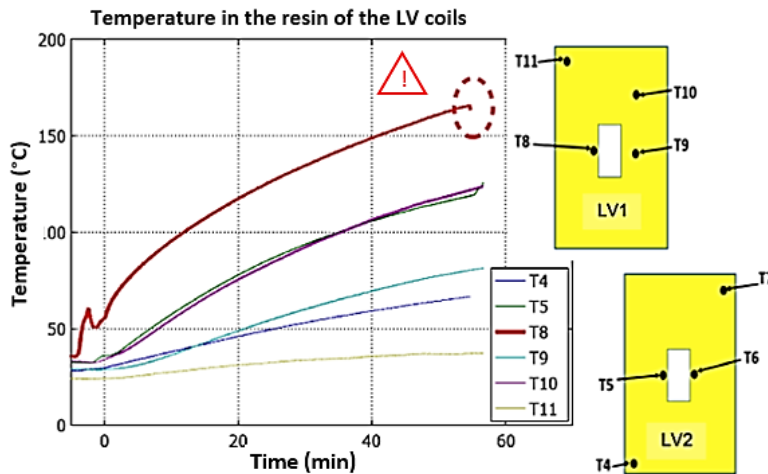


Fig.14. Temperature measurements made at several points inside the coil resin.

The overeating observed during this test comes from the design habits that have not been sufficiently adapted to the hot-core transformer. The prototype has been designed with 1 mm thick air layers between the core and the coils. During the realization of the prototype these distances have not been respected with enough accuracy. Consequently, Hot spots appear at the coil inner surfaces at several points. Despite the fault observed during the test at low-load, the experimental investigations have been carried on with a lower input voltage and high currents in coils.

3. Test at low voltage and high current

This test is made for analyzing the behavior of SST cell at high currents. The testing circuit is the same (Fig. 11). The supply voltage is set to 280 V DC ; the load is a high-power resistance of 0.5Ω . The recorded voltages and currents are presented in Fig. 15 for an operating point corresponding to $\varphi = 60^\circ$. The currents curves are in

green (i_1) and red (i_2), with a vertical scale on the right; the voltage curves are in blue (v_1) and black (v_2) with a vertical scale on the left.

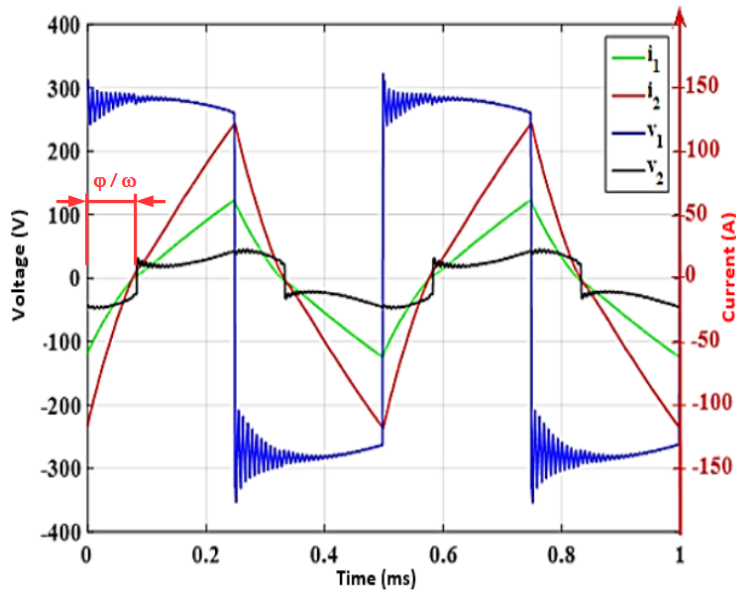


Fig.15. Voltages and currents recorded during the test at low voltage and high current for $\varphi = 60^\circ$.

The current waveforms are very near the theoretical ones (Feng B. et al, 2014). The small difference is due to the influence of the non-infinite value of the capacitance C_B . The fast damped oscillation observed on (v_1) are due to the connections of the IGBT bridges made by short wires, they can be reduced using busbar connections. For this operating point, the current RMS values are $I_{1RMS} = 35.1 A$ and $I_{2RMS} = 68.5 A$, which corresponds to a DC output current in the load of 59 A and a DC input current of 12.5 A. At this command angle φ , the power factor of the transformer is only 0.36. The low power factor for high values of the command angle φ is a classical limit of SSTs. However, this low power factor corresponds to an exchange of energy between the input capacitance C_A and the transformer leakage inductance. The corresponding additional losses remain low when the coil AC resistances are low.

VI. NEW THERMAL DESIGN

The test at low load has clearly pointed out a thermal problem. The transformer design must be improved for limiting the heat transfer from the hot central core to the coils. This transfer depends on the thermal resistances highlighted in red in Fig. 16; they must be increased.

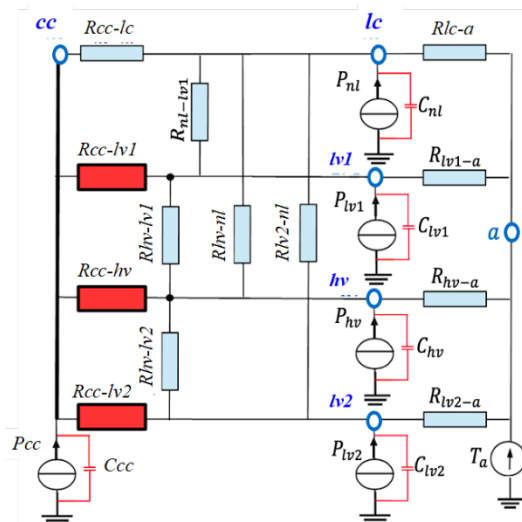


Fig. 16. Critical thermal resistances (in red) limiting the temperature difference between the central core and the coils.

The new proposed design consists in adding a thermal insulating layer between the central leg of the core and the 3 coils. The core central leg is placed in a high temperature ceramic fiber fabric able to operate up to very high

temperatures (1260°C). Such fabrics are manufactured from alumina-silica ceramic fiber (70%) and other inorganic materials. They can be supplied in the form of strips or sheaths of several diameters (www.final-materials.com). The thin ceramic fibers inside the fabric provide a standstill air layer between the core and the coils that is used as a thermal insulating layer. Let us consider a layer of 2 mm thick high temperature fabric for calculating the new values of the critical thermal resistances (Table V).

Table V. Estimation of critical thermal resistances with a thermal insulation layer between the central core and the coils.

Material	R_{cc-hv} Central core – HV coil (K/W)	$R_{cc-lv1,2}$ Central core – LV coils (K/W)
Air inside the high temperature fabric	4.29	10.6
Epoxy resin	0.42	0.21
Total	4.71	10.81

The equivalent circuit of Fig.16 is used for evaluating the performance of a SST cell made with the new thermal design. The sources representing the core and copper losses are determined at the operating point defined by the two tests presented above. The RMS currents of the second test associated to the coil AC resistances measured at 2 kHz yield the copper losses at 20°C (502 W in the HV coil and 231 W in each LV coil). The first test at low load gives the specific core losses at 20°C (87 W/kg) and the initial losses in each part of the core. The SPICE simulation of the equivalent circuit, run with these initial data, yields the transient temperatures of Fig. 17. Table VI gives the core losses at the initial and final temperatures.

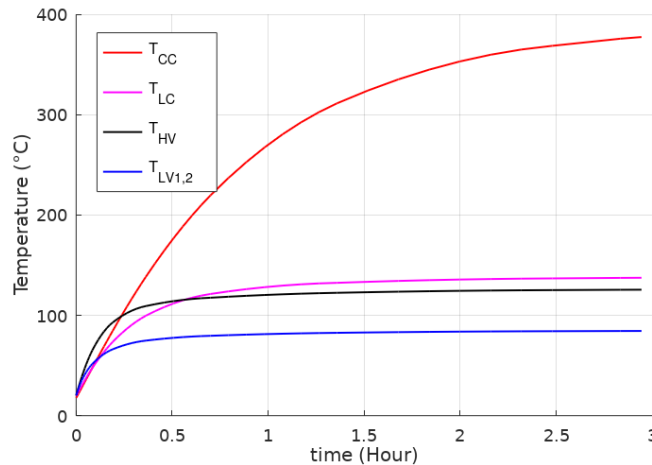


Fig.17. Temperature estimations (central core T_{nc} , lateral core T_{nl} , HV coil T_{HV} and LV coil T_{LV1} and T_{LV2}).

Table VI. Core losses at the initial and final temperatures.

	Mass (kg)	Core losses at 20°C (W)	Final temperature (°C)	Specific losses variations (W/kg)	Losses variations (W)	Losses at the final temperature (W)
Central Core (CC)	2.05	178	378	-2.1	-51.3	126.7
Lateral cores (LC)	3.58	311	141	-8.47	-30.3	280.7
Total	5.63	489			-81.6	407.4

The inorganic insulating layer around the central core brings a global reduction of 81.6W (16.7%) of the core losses comparing to a core operating at 20°C. This 2 mm thick layer reduces a little the area of the core windows available for the coils. For the transformer of the prototype this reduction is 4.2 cm², which represents only 2.9% of the initial area.

Because of the symmetry of the equivalent circuit, the temperatures predictions of the two LV coils are identical. At steady state, the predicted temperature are 126°C for the HV coil and 87°C for the LV one. These temperatures are much lower than the limit imposed by a standard class F electrical insulation system, which is 155°C for a live time of 20 000 h. The coils can be made with classical Litz wires able to provide a low AC resistance at the operating frequency.

The tests presented in sections V.2 and V.3 can be extrapolated considering the new thermal design. With the same coil cooling system (heatsink in an air flow) and a ceramic fiber fabric around the central core, the extrapolation gives a transmitted power of 19 kW.

VIII. CONCLUSION

The paper presents a possible new design for high power SST cells operating at a medium frequency, in the kHz range. The proposed design is based on a GOES wound core made of thin strips. In such a core, the magnetic field vector is in the rolling direction at any point. Consequently, it is possible to benefit of the excellent characteristics of the material in its easy magnetization direction (high saturation flux density and high permeability). Moreover, the GOES can operate a very high temperature, up to $500^{\circ}C$, when the designer accepts a small reduction of the saturation flux density. At high temperatures the cores losses are lower because of the natural increase of the material resistivity. The paper proposes also a nodal thermal equivalent circuit very helpful for the high temperature core transformer design.

Comparing with the other available technologies, with GOES wound cores it is possible to build longer cores with larger windows giving more room for coils. However, a thermal insulation between the core and the coils must be added for keeping a standard electrical insulation system. The proposed new design consists in adding an inorganic fabric, made with ceramic fiber, between the core and the coils. With the proposed design, an efficient thermal management and coils made with Litz wires, the power density of the medium frequency transformer can reach $3.3\text{ kVA}/dm^3$ and an efficiency of 96%.

The grain oriented electrical steel is now a soft magnetic material that benefits of a long industrial experience and constant improvements during last decades. The production industrial process is now optimized and the global production environmental footprint is as low as possible. The very stable crystalline structure of this electrical steel provides constant characteristics and long-life expectancies. This material is now available in wide and thin strips that made it possible the design of large cores for high power medium frequency transformers at a reasonable cost.

IX. ACKNOWLEDGMENT

This work is funded by thyssenKrupp Electrical Steel.

REFERENCES

- Ababsa M.L and Ninet O. and Velu G. and Lecoite J.P. (2018), "High-Temperature Magnetic Characterization Using an Adapted Epstein Frame," *IEEE Transactions on Magnetics*, vol. 54, pp. 1-6, 6 2018. DOI: 10.1109/TMAG.2018.2811727.
- Basso V. et al. (1997), "Power losses in magnetic laminations with hysteresis: Finite element modeling and experimental validation," *J. Appl. Phys.*, vol. 81, no. 8, pp. 5606–5608, 1997.
- Beckley Ph. (2000), "Electrical Steels - A Handbook for Producers and Users", Publisher, Newport, South Wales : European Electrical Steels, 2000.
- Bertotti G. (1988), "General properties of power losses in soft ferromagnetic materials," *IEEE Trans. Magn.* vol. MAG-24, no. 1, pp. 621–630, Jan. 1988.
- Bhuyan A. and Mor R. and Morshui P. and Montanari G.C. and Erinkveld W. (2014), "Analysis of the arcing process in on-load tap changers by measuring the acoustic signature," in 2014 IEEE Electrical Insulation Conference (EIC), pp. 193–197, June 2014.
- Cheng Z. et al. (2014), "Modeling of magnetic properties of GO electrical steel based on Epstein combination and loss data weighted processing," *IEEE Trans. Magn.*, vol. 50, no. 1, 2014, Art. no. 6300209.
- Du Y. and Baek S. and Bhattacharya S. and Huang A.Q. (2010), "High-voltage high-frequency transformer design for a 7.2 kV to 120V/240V 20kVA solid state transformer", *IECON 2010-36th Annual Conference on IEEE Industrial Electronics Society (pp. 493-498)*. IEEE. DOI: 10.1109/IECON.2010.5674828.
- Dujic D. and Kieferndorf F. and Canales F. and Drofenik U.(2012), "Power electronic traction transformer technology," in *Proceedings of The 7th International Power Electronics and Motion Control Conference*, 2012. DOI: 10.1109/IPEMC.2012.6258820
- Dujic, D., Kieferndorf, F. and Canales, F., (2012). "Power electronic transformer technology for traction applications—an overview". *Electronics*, 16(1), pp.50-56. DOI: DOI:10.7251/ELS1216050D.
- Elrajoubi A.M. and Ang S.S. (2019), "High-frequency transformer review and design for low-power solid-state transformer topology", *IEEE Texas Power and Energy Conference (TPEC)* (pp. 1-6). IEEE. DOI: 10.1109/TPEC.2019.8662131.
- Feng B. and Wang Y., and Man J. (2014), "A novel dual-phase-shift control strategy for dual active-bridge dc-dc converter," in *IECON-40th Annual Conference of the IEEE Industrial Electronics Society*. IEEE, 2014, pp. 4140–4145.

- Garcia-Bediaga A. and Villar I. and Rujas A. and Mir L. and Rufer, A. (2016), "Multiobjective optimization of medium-frequency transformers for isolated soft-switching converters using a genetic algorithm. *IEEE Transactions on Power Electronics*, 32(4), pp.2995-3006. DOI: 10.1109/TPEL.2016.2574499.
- Hamdinou S. (2019), "Potentiel des aciers électriques à grains orientés pour la réalisation de transformateurs compacts à forte densité de puissance", Ph.D thesis, Artois University, December 2019.
- Huber J.E. and Kolar J.W. (2014), "Volume/weight/cost comparison of a 1MVA 10 kV/400 V solid-state against a conventional low-frequency distribution transformer," in *2014 IEEE Energy Conversion Congress and Exposition (ECCE)*, 2014. DOI: 10.1109/ECCE.2014.6954023.
- Ichou H. and Roger D. and Rossi M. and Belgrand T. (2019), "Assessments of High-Power Solid State Transformers based on Grain-Oriented magnetic cores," in *2019 IEEE 12th International Symposium on Diagnostics for Electrical Machines, Power Electronics and Drives (SDEMPED)*, 2019. DOI: 10.1109/DEMPED.2019.8864806.
- Ichou H. and Roger D. and Rossi M. and Belgrand T. and Lemaitre R. (2020), "Assessment of a grain oriented wound core transformer for solid state converter," in *2020 Journal of Magnetism and Magnetic Materials - JMMM 504*, 2020. DOI:10.1016/j.jmmm.2020.166658.
- Ichou H. (2020) "Conception de « Solid-State Transformers (SST) » de fortes puissances construits autour de transformateurs dotés de noyaux enroulés en acier électrique à grains orientés", Ph.D thesis, Artois University, December 2020.
- IEC 60404-1-1 standard (2004), "Magnetic materials. Classification – Surface insulations of electrical steel sheet, strip and laminations", April 2004.
- Lemaitre, R. and Belgrand, T. (2014), "Matériaux magnétiques doux cristallins. Acier électrique à grains orientés". *Techniques de l'ingénieur, energies-th4, matériaux magnetiques en electrotechnique 42259210 / D2124*.
- McLyman C. W. T. (2017), "Transformer and inductor design handbook". CRC press, 2017.
- Messal O. and Sixdenier F. and Morel L. and Burais N., "Temperature dependent extension of the Jiles–Atherton model: Study of the variation of microstructural hysteresis parameters," *IEEE Trans. Magn.*, vol. 48, no. 10, pp. 2567–2572, Oct. 2012.
- Nan C. and Ayyanar R. (2013), "Dual active bridge converter with PWM control for solid state transformer application," in *2013 IEEE Energy Conversion Congress and Exposition*, pp. 4747–4753.
- Ozdemir S. and Balci, S. and Altin, N. and Sefa, I. (2017). "Design and performance analysis of the three-level isolated DC-DC converter with the nanocrystalline core transformer" *International Journal*
- Rodriguez-Sotelo D. and Martin A. and Rodriguez-Licea M.A. and Allan G. and Soriano-Sanchez A.G and Espinosa-Calderon A. and Perez-Pinal F J. (2020), "Advanced Ferromagnetic Materials in Power Electronic Converters: A State of the Art", IEEE Access, special section on evolving technologies in energy storage systems for energy systems applications, March 2020, DOI 10.1109/ACCESS.2020.2982161.
- Steimel, A. (1996), "Electric railway traction," *IEEE Industry Applications Magazine*, 1996, 2, 6-17.
- Thalheim, J. (2008), "Chipset for Flexible and Scalable High-Performance Gate Drivers for 1200 V-6500 V IGBTs," *20th International Symposium on Power Semiconductor Devices and IC's*, 2008, 197-200.
- Wang, K., Lei, Q. and Liu, C. (2017), "Methodology of reliability and power density analysis of SST topologies," In *2017 IEEE Applied Power Electronics Conference and Exposition (APEC)* (pp. 1851-1856), March 2017. DOI: 10.1109/APEC.2017.7930950.
- www.infineon.com/cms/en/product/
- www.final-materials.com/fr/23-fibre-ceramique-mono-filament
- Xia Z. and Kang Y. and Wang Q. (2008), "Developments in the production of grain-oriented electrical steel," *Journal of Magnetism and Magnetic Materials*, vol. 320, no. 23, pp. 3229 – 3233, Dec. 2008.
- Zhao C. and Weiss M. and Mester A. and Lewdeni-Schmid S. and Dujic D. and Steinke J. K and Chaudhuri T. (2012), "Power electronic transformer (PET) converter: Design of a 1.2MW demonstrator for traction applications," in *International Symposium on Power Electronics Power Electronics, Electrical Drives, Automation and Motion*, 2012. DOI: 10.1109/SPEEDAM.2012.6264496.